Research Article

INTERNATIONAL JOURNAL OF ADVANCED ROBOTIC SYSTEMS

International Journal of Advanced Robotic Systems
March-April 2021: 1–14

DOI: 10.1177/17298814211992963
journals.sagepub.com/home/arx
SAGE

Inverse and forward kinematics and workspace analysis of a novel 5-DOF (3T2R) parallel–serial (hybrid) manipulator

Anton Antonov[1], Alexey Fomin[1], Victor Glazunov[1], Sergey Kiselev[1] and Giuseppe Carbone[2]

Abstract

The proposed study provides a solution of the inverse and forward kinematic problems and workspace analysis for a five-degree-of-freedom parallel–serial manipulator, in which the parallel kinematic chain is made in the form of a tripod and the serial kinematic chain is made in the form of two carriages displaced in perpendicular directions. The proposed manipulator allows to realize five independent movements—three translations and two rotations motion pattern (3T2R). Analytical relationships between the coordinates of the end-effector and five controlled movements provided by manipulator's drives (generalized coordinates) were determined. The approach of reachable workspace calculation was defined with respect to available design constraints of the manipulator based on the obtained algorithms of the inverse and forward kinematics. Case studies are considered based on the obtained algorithms of inverse and forward kinematics. For the inverse kinematic problem, the solution is obtained in accordance with the given laws of position and orientation change of the end-effector, corresponding to the motion along a spiral-helical trajectory. For the forward kinematic problem, various assemblies of the manipulator are obtained at the same given values of the generalized coordinates. An example of reachable workspace designing finalizes the proposed study. Dimensions and extreme values of the end-effector orientation angles are calculated.

Keywords

5-DOF manipulator, parallel–serial (hybrid) manipulator, three translations and two rotations motion pattern (3T2R), inverse and forward kinematics, reachable workspace, MATLAB simulation, CAD modeling

Date received: 19 October 2020; accepted: 14 January 2021

Topic Area: Service Robotics
Associate Editor: Marco Ceccarelli
Topic Editor: Marco Ceccarelli

Introduction

The performance and efficiency of robotic, technological, medical, and research devices mainly depend on the mechanical systems based on which they are designed. Currently, parallel mechanical systems are widely used to realize various operations. These systems provide high performance in load capacity, accuracy, and speedwork.[1,2] However, they do not always fully meet practical

[1] Mechanisms Theory and Machines Structure Laboratory, Mechanical Engineering Research Institute of the Russian Academy of Sciences (IMASH RAN), Moscow, Russia
[2] Department of Mechanical, Energy and Management Engineering (DIMEG), University of Calabria, Rende, Italy

Corresponding author:
Alexey Fomin, Mechanisms Theory and Machines Structure Laboratory, Mechanical Engineering Research Institute of the Russian Academy of Sciences (IMASH RAN), Moscow 101000, Russia.
Email: alexey-nvkz@mail.ru

requirements due to restricted sizes of their working zones in comparison with systems having serial structure. This limits the practical application of parallel mechanical systems. In this regard, the mechanical systems that simultaneously include parallel and serial kinematic chains are quite promising in terms of advanced functional properties. Mechanical systems built on this principle are rated as hybrid systems.[3–5]

Currently, many hybrid mechanisms, manipulators, and robots are known, including those with parallel–serial structure and providing increased rigidity, speedwork, extended sizes of working zones, and other important functional properties. Among such mechanical systems are five-degree-of-freedom (5-DOF) Cassino Hybrid Manipulator, which consists of parallel part in the form of a 3-DOF tripod, on the platform of which a 2-DOF telescopic arm is mounted;[6] hybrid robot manipulator, which is used for propeller grinding;[7] 5-DOF manipulator Georg V including parallel chain—a tripod, with an additional serial chain—a two-axis wrist joint;[8] 10-DOF industrial manipulator designed for studying the feasibility of loading packages inside a trailer (UPSarm);[9] 6-DOF manipulator, which consists of a 3-DOF planar parallel part and a 3-DOF serial part, that is designed as a robotic arm;[10] 5-DOF mechanism for positioning a laser head composed of a parallel chain in the form of a planar mechanism and a serial chain in the form of a spatial mechanism;[11] 5-DOF Parallel Mechanism—Wrist Mechanism manipulator, which includes a parallel part providing displacements along three coordinate axes and a wrist (serial) part providing two rotations;[12] 6-DOF modular manipulator for robotized deburring applications, which includes a 3-RRR chain having parallel structure and a PRR arm having serial structure;[13] 5-DOF micromanipulator designed for ophthalmic surgery, which includes two parallel kinematic chains and one serial chain—needle slider;[14,15] five-axis (5-DOF) machine tool, which has a 2-DOF parallel part and 3-DOF serial part;[16] 6-DOF forging mechanism with application to heavy-duty manipulations;[17] 6-DOF micromanipulator consists of two compliant parallel kinematic chains—a 3-RRR chain and a 3-RPS chain;[18] mobile robot, which includes a planar parallel chain in the form of star-triangle mechanism and a serial puma-type manipulator arm;[19] 4-DOF haptic micromanipulator utilizing a planar 3-PRR parallel mechanism (3-DOF mechanism) and a planar 1-DOF modular bridge mechanism;[20] 5-DOF machine tool, which consists of a 3-DOF parallel mechanism and a 2-DOF serial mechanism;[21] 5-DOF (with 3T2R motion pattern) polishing machine, which includes a 3-DOF parallel mechanism for vertical motion and XY rotations and a 2-DOF serial mechanism for XY positioning;[22] humanoid arm, which consists of a serial chain of shoulder, elbow, and wrist joints and a 3-UPS/S parallel mechanism prototyping a wrist joint;[23] VERNE machine, which is five-axis machine tool designed with a 3-DOF parallel module having three nonidentical legs and a 2-DOF serial kinematic chain—tilting table;[24] 6-DOF machine tool, which includes a 3-PRS parallel chain, serial chain with XY translations, and an end-effector with additional independent rotation around its axial axis;[25] and worm-like robot, which designed with a 3-RPS and a 3-SPR parallel modules.[26]

Structure, analysis, and control algorithms of hybrid mechanical systems, including parallel–serial systems, are presented in the works of Shahinpoor[5] (automated construction of hybrid manipulator for crane-type applications), Romdhane[27] (6-DOF manipulator with two platforms which stay on three legs), Huang and Ling[28] (6-DOF hybrid manipulator, where 3-DOF serial actuated module is mounted on a moving platform of another 3-DOF parallel actuated chain), Zanganeh and Angeles[29] (hybrid hand controller that includes RSRS parallel module and wrist serial module), Tanev[30] (similar to 6-DOF manipulator with two platforms shown in Romdhane[27] but having different structure of legs: lower parallel part has three legs with SPS, RPS, and RPR structure; upper part has two identical legs with SPS and one with RRR structure), Zheng et al.[31] (hybrid manipulator that includes two 3-UPU parallel kinematic chains), Dyashkin-Titov et al.[32] (6-DOF parallel–serial manipulator based on parallel chain—tripod and serial chain—gripping device), Gallardo-Alvarado[33] (6-DOF hybrid manipulator that includes 3-translational-DOF lower and 3-rotational-DOF upper parallel mechanisms, where the lower mechanism consists of 3-SPU independent (actuated) and two passive kinematic chains, when the upper mechanism consists of 3-UPS and 1-S chains), Hu et al.[34] (hybrid manipulator 5×(PS-RPS-SPS) that includes five modules of three-legged manipulators with kinematic chains PS, RPS, and SPS), Bandyopadhyay and Ghosal[35] (6-DOF 3-RRRS hybrid manipulator), Zhang et al.[36] (5-DOF parallel–serial manipulator, where parallel part consists of 2-UPU and SP kinematic chains and serial part consists of RR kinematic chain), Wang et al.[37] (3-DOF "Active Dynamic Balancing Mechanism (ADBM)" that includes 2-PRR parallel chains and serial chain in the form of a rotational platform), Zeng and Fang[38] (3-DOF parallel–serial mechanical structure with spatial translational motion), Milutinovic and Slavkovic[39] (5-DOF parallel–serial machine tool that includes 3-DOF tripod as a parallel kinematic chain and 2-DOF wrist as a serial kinematic chain), Fan et al.[40] (5-DOF parallel–serial machine tool that consists of a 3-DOF spindle platform and 2-DOF X–Y table), Zhang and Meng[41] (5-DOF parallel–serial mechanism composed of two identical 3-UPU parallel mechanisms and two gripping modules), Lu et al.[42] (2×(RPS-SPR-UPS-SPU) hybrid manipulator), and Ibrahim and Khalil[43] (hybrid robots which are constructed by serially connected parallel modules).

The studies listed above provide mechanisms, manipulators, and robots with advanced functional characteristics and oriented for specific operations. Despite this, there is a challenge to improve their designs, particularly, to enlarge their workspaces. Therefore, the proposed study presents a

novel 5-DOF parallel–serial (hybrid) manipulator with 3T2R motion pattern, which provides large workspace dimensions. The study aims to develop algorithms of inverse and forward kinematics and reachable workspace construction of the manipulator.

The remaining part of this study is organized as follows. Section "Manipulator architecture" considers geometry of the manipulator and its mobility with respect to the integrated kinematic chains. A computer-aided design (CAD) model of the manipulator created on the basis of its structural scheme is presented here. Section "Kinematic analysis of the manipulator" presents algorithms for solving the inverse and forward kinematic problems, where the analytical relationships between the coordinates of the end-effector and five controlled movements in the actuators (generalized coordinates) are determined. This section also provides an approach of reachable manipulator's workspace calculation. Section "Examples of kinematic problems solution and workspace construction" is focused on the case study based on the developed kinematic algorithms: for the inverse problem—when the end-effector moves along a spiral-helical trajectory; for the forward problem—when different assemblies of the manipulator are defined for the same values of the generalized coordinates. Also, an example of reachable workspace construction is presented. The article ends with section "Conclusions," which presents the findings of the conducted study.

Manipulator architecture

Let's discuss structural scheme of the investigated manipulator, which is shown in Figure 1. Therein, 1 is the fixed link, on which three kinematic chains are mounted. Each chain is equipped with an actuator providing displacement q_1, q_2, or q_3. One of these chains is comprised of links 2–3, where 2 is the driving link and 3 is the spider of the universal (cardan) joint, and the other two chains are comprised of links 4–5, where 4 is the driving link and 5 is the leg.

Each of the three chains mounted on the fixed link is coupled with movable frame 6, on which a carriage is located, formed by links 7 and 8 rigidly connected to each other. Therein, an additional carriage 9 is coupled with link 8. Thus, both carriages provide displacements in perpendicular directions in the plane of frame 6 and have actuators providing displacements q_4 and q_5. Output element 10 is mounted on carriage 9, so these two links form the manipulator's end-effector.

Kinematic pairs 1–2, 1–4, 6–7, and 8–9 are prismatic; pairs 2–3 and 3–6 are rotational; pairs 4–5 and 5–6 are spherical. The manipulator includes a spatial part with parallel structure (links 1–6) and a planar part with serial structure (links 7–9).

Kinematic chain 1–2–3 in the parallel part provides frame 6 with three DOFs due to having the universal joint. The joint imposes three following constraints: the first one is on the rotation of frame 6 around the axis perpendicular to the spider plane, and two others are on the translations in any directions perpendicular to this axis. Therefore, three actuators providing displacements q_1, q_2, and q_3 are required for positioning frame 6 in space. The remaining two chains 1–4–5, located in the parallel part of the manipulator, do not impose any constraints on the movement of frame 6 and the end-effector. A passive mobility appears in each of chains 1–4–5: the rotation of legs 5 around their longitudinal axes. Such mobility does not affect the movement of frame 6 and the end-effector.

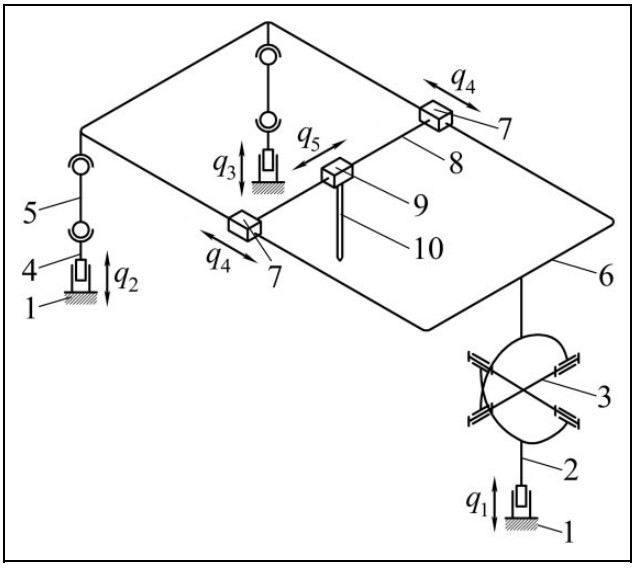

Figure 1. Structural scheme of the 5-DOF (3T2R) parallel–serial (hybrid) manipulator.

The planar part with the serial structure provides the manipulator with two additional DOFs—translational displacements in perpendicular directions in the plane of frame 6, determined by parameters q_4 and q_5. Thus, the positioning of the end-effector is realized by five actuators providing displacements q_1, q_2, q_3, q_4, and q_5; 3T2R motion pattern of the end-effector is provided as follows: the parallel part provides one translation and two rotations motion pattern (1T2R) and the serial part provides two translations (2T).

One should note that 3T2R motion pattern can degenerate in singular positions. For example, if the manipulator is in the position where the plane of spider 3 is parallel to the axis of displacement q_1, one translational DOF is lost. In this case, displacements q_1 and q_3 will correspond to the displacement along one coordinate of the end-effector.

The mobility of this manipulator can be verified using structural formulae. The mobility of the parallel part is determined by the following formula for spatial kinematic chains

$$W = 6n - 5p_5 - 4p_4 - 3p_3 - 2p_2 - p_1, \qquad (1)$$

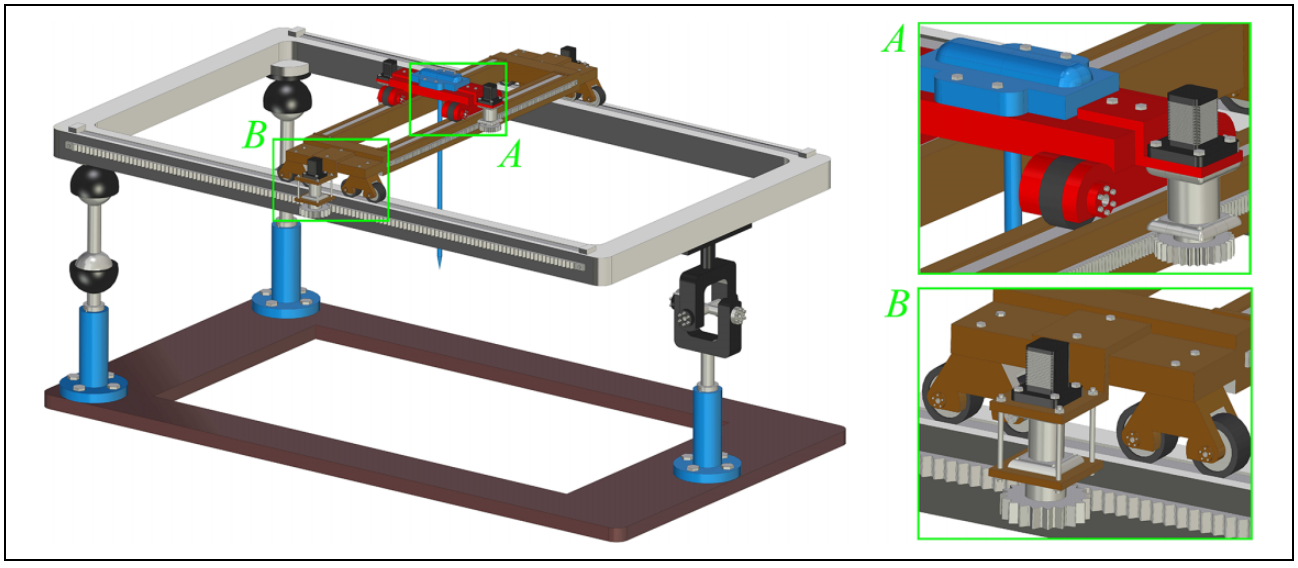

Figure 2. CAD model of the 5-DOF (3T2R) parallel–serial (hybrid) manipulator.

where W is the mobility of kinematic chains defining its number of DOFs; n is the number of movable links of a kinematic chain; p_5, p_4, p_3, p_2, and p_1 are the numbers of 1-, 2-, 3-, 4-, and 5-DOF kinematic pairs.

Having parameters $n = 7$, $p_5 = 5$, and $p_3 = 4$ of the parallel part of the manipulator, it comes from (1) that $W = 5$. Excluding two passive mobilities of legs 5, three DOFs remain for the parallel part, that is, $W = 3$.

The mobility of the serial part can be defined by the following formula for planar kinematic chains

$$W = 3n - 2p_5 - p_4. \tag{2}$$

Having parameters $n = 2$ and $p_5 = 2$ of the serial part of the manipulator, it follows from (2) that $W = 2$. Thus, the overall mobility of the manipulator is determined by summing the results obtained by (1) and (2), and with the exclusion of two mobilities in the parallel part, the overall mobility becomes equal to five.

Based on the structural scheme of the manipulator shown in Figure 1, its detailed CAD model was developed. It is shown in Figure 2. The carriages provide the movement of links along frame 6 in perpendicular directions. Each carriage has two actuators on both sides.

The application of this manipulator can be associated with the manufacture and processing of machine components having complex shapes, as well as mechanical elements, in which the longitudinal dimension exceeds the transverse one. The application of this manipulator can also be associated with performing surgical operations and research procedures.

Kinematic analysis of the manipulator

Consider kinematic analysis of the manipulator, which consists, first of all, in solving inverse and forward position problems. The solution of these problems is in searching the relationships between the coordinates of the end-effector and the controlled movements in the manipulator drives, which are chosen as generalized coordinates. Therein, the inverse problem aims to calculate the generalized coordinates for specified end-effector coordinates, and the forward problem is aimed at determining the position and orientation of the end-effector for specified generalized coordinates.

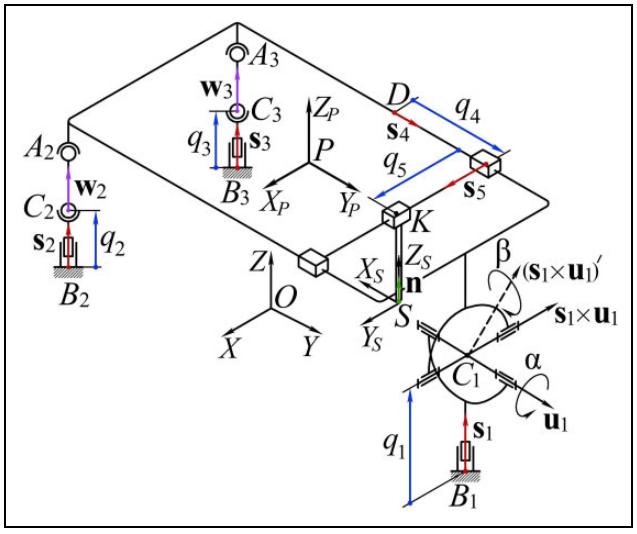

Figure 3. Toward kinematic analysis of the 5-DOF (3T2R) parallel–serial (hybrid) manipulator.

The position of the end-effector can be described by the Cartesian coordinates of any its points, for example, point S (Figure 3). These coordinates can be represented as vector $\mathbf{p}_S$, which determines the position of point S in global coordinate system $OXYZ$.

Let's locate coordinate system $SX_SY_SZ_S$ at point S of the end-effector in such a way that its Z_S axis is directed along

the axial axis of output element 10—unit vector $\mathbf{n}$ (Figure 3). Since the manipulator's end-effector has five DOFs (three translational and two rotational), the coordinates of vector $\mathbf{n}$ uniquely determine the orientation of the end-effector. The directions of two remaining axes (X_S and Y_S) of coordinate system $SX_SY_SZ_S$ can be arbitrarily selected. The orientation of the end-effector can also be specified by using rotation matrix $\mathbf{R}_S$ of coordinate system $SX_SY_SZ_S$ relative to system $OXYZ$, where one of the columns is vector $\mathbf{n}$.

The generalized coordinates of the manipulator can be written as vector $\mathbf{q}$

$$\mathbf{q} = [\,q_1 \quad q_2 \quad q_3 \quad q_4 \quad q_5\,]^{\mathrm{T}}, \tag{3}$$

where values $q_1 \ldots q_5$ correspond to the displacements in actuated kinematic pairs (Figure 3).

Consider next the features of solving inverse and forward kinematic problems for the discussed 5-DOF manipulator.

Inverse kinematics solution

The solution of the inverse problem consists in determining generalized coordinates vector $\mathbf{q}$ for specified vector $\mathbf{p}_S$ describing the position of the end-effector, and specified matrix $\mathbf{R}_S$ (vector $\mathbf{n}$) describing its orientation. The methodology for solving this problem can be presented as follows.

Let's attach coordinate system $PX_PY_PZ_P$ to frame 6. Its origin, point P, as well as the directions of the axes can be arbitrarily chosen (Figure 3). The orientation of the end-effector relative to frame 6 is kept constant since the movement of the end-effector relative to frame 6 is realized by two prismatic kinematic pairs 6–7 and 8–9. In this regard, the following ratio can be written

$$\mathbf{n} = \mathbf{R}_P\mathbf{n}^P, \tag{4}$$

where $\mathbf{R}_P$ is the rotation matrix defining the orientation of coordinate system $PX_PY_PZ_P$ relative to system $OXYZ$; $\mathbf{n}^P$ are the coordinates of vector $\mathbf{n}$ relative to coordinate system $PX_PY_PZ_P$.

The components of vector $\mathbf{n}^P$ are constant and determined only by the manipulator's design and by the selected direction of the axes of coordinate system $PX_PY_PZ_P$. Then rotation matrix $\mathbf{R}_P$ can be defined as follows

$$\mathbf{R}_P = \mathbf{R}_{C1}\mathbf{R}_\alpha\mathbf{R}_\beta\mathbf{R}_P^{C1}, \tag{5}$$

where rotation matrices $\mathbf{R}_{C1}$, $\mathbf{R}_\alpha$, $\mathbf{R}_\beta$, and $\mathbf{R}_P^{C1}$ have the following meaning:

(1) Matrix $\mathbf{R}_{C1}$ determines the orientation of the coordinate system built at the center of universal joint 2–3, point C_1 (Figure 3), relative to global system $OXYZ$, and it can be composed as follows

$$\mathbf{R}_{C1} = [\,\mathbf{u}_1 \quad \mathbf{s}_1 \times \mathbf{u}_1 \quad \mathbf{s}_1\,], \tag{6}$$

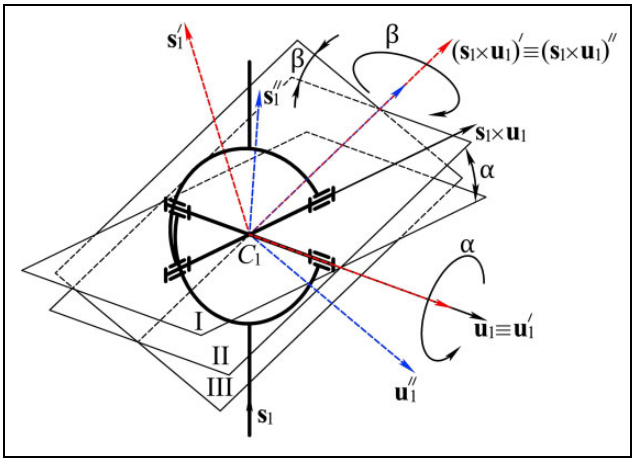

Figure 4. Links movements (rotations) in 2-DOF universal joint.

where $\mathbf{u}_1$ is the unit vector directed along the axis of the rotational pair in universal joint 2–3; $\mathbf{s}_1$ is the unit vector directed along the axis of prismatic pair 1–2 and corresponding to the direction of generalized coordinate q_1 (Figure 4).

All the components of matrix $\mathbf{R}_{C1}$ are constants since the direction of vectors $\mathbf{u}_1$ and $\mathbf{s}_1$ depends only on the manipulator's design.

(2) Matrix $\mathbf{R}_\alpha$ corresponds to rotation at angle α around axis $\mathbf{u}_1$ in the universal joint

$$\mathbf{R}_\alpha = \begin{bmatrix} 1 & 0 & 0 \\ 0 & \cos\alpha & -\sin\alpha \\ 0 & \sin\alpha & \cos\alpha \end{bmatrix}. \tag{7}$$

(3) Matrix $\mathbf{R}_\beta$ corresponds to rotation at angle β around axis $(\mathbf{s}_1\times\mathbf{u}_1)'$ in the universal joint

$$\mathbf{R}_\beta = \begin{bmatrix} \cos\beta & 0 & \sin\beta \\ 0 & 1 & 0 \\ -\sin\beta & 0 & \cos\beta \end{bmatrix}. \tag{8}$$

(4) Matrix $\mathbf{R}_P^{C1}$ defines the orientation of coordinate system $PX_PY_PZ_P$ of frame 6 relative to the coordinate system, the axes of which are directed along vectors $\mathbf{s}_1''$, $(\mathbf{s}_1\times\mathbf{u}_1)''$, and $\mathbf{u}_1''$ (Figure 4). The coordinates of these vectors relative to coordinate system $PX_PY_PZ_P$ remain constant since the upper part of universal joint 2–3 and frame 6 form an entire link. Consequently, all the components of matrix $\mathbf{R}_P^{C1}$ are constants and are determined by the manipulator's design. Next, substitute (5) in (4) and rewrite the obtained solution as:

$$\mathbf{n}_1 = \mathbf{R}_\alpha\mathbf{R}_\beta\mathbf{n}_2, \tag{9}$$

where

$$\mathbf{n}_1 = \mathbf{R}_{C1}^{\mathrm{T}}\mathbf{n}, \mathbf{n}_2 = \mathbf{R}_P^{C1}\mathbf{n}^P. \tag{10}$$

Components of vector $\mathbf{n}_1$ are given parameters in solving inverse kinematics, and components of vector $\mathbf{n}_2$ are constants. Let's expand expression (9) with respect to (7) and (8):

$$\begin{bmatrix} n_{1x} \\ n_{1y} \\ n_{1z} \end{bmatrix} = \begin{bmatrix} \cos\beta & 0 & \sin\beta \\ \sin\alpha\sin\beta & \cos\alpha & -\sin\alpha\cos\beta \\ -\cos\alpha\sin\beta & \sin\alpha & \cos\alpha\cos\beta \end{bmatrix} \begin{bmatrix} n_{2x} \\ n_{2y} \\ n_{2z} \end{bmatrix}, \quad (11)$$

where n_{1x}, n_{1y}, n_{1z} and n_{2x}, n_{2y}, n_{2z} are components of vectors $\mathbf{n}_1$ and $\mathbf{n}_2$.

Expression (11) can be used to determine angles α and β. For example, the relationship for calculating angle β can be obtained from the first line of expression (11)

$$n_{2x}\cos\beta + n_{2z}\sin\beta = n_{1x}, \quad (12)$$

from which

$$\beta = \pm\arccos\frac{n_{1x}}{\sqrt{n_{2x}^2 + n_{2z}^2}} + \arctan\frac{n_{2z}}{n_{2x}}. \quad (13)$$

As far as rotation matrices are orthogonal, expression (12) can be rewritten as follows

$$\begin{bmatrix} n_{2x} \\ n_{2y} \\ n_{2z} \end{bmatrix} = \begin{bmatrix} \cos\beta & \sin\alpha\sin\beta & -\cos\alpha\sin\beta \\ 0 & \cos\alpha & \sin\alpha \\ \sin\beta & -\sin\alpha\cos\beta & \cos\alpha\cos\beta \end{bmatrix} \begin{bmatrix} n_{1x} \\ n_{1y} \\ n_{1z} \end{bmatrix}. \quad (14)$$

The expression for calculating angle α can be similarly composed from the second line of expression (14)

$$n_{1y}\cos\alpha + n_{1z}\sin\alpha = n_{2y}, \quad (15)$$

from which

$$\alpha = \pm\arccos\frac{n_{2y}}{\sqrt{n_{1y}^2 + n_{1z}^2}} + \arctan\frac{n_{1z}}{n_{1y}}. \quad (16)$$

Expressions (13) and (16) allow finding the values of angles α and β in universal joint 2–3. The selection of the sign in these expressions is determined by the manipulator's design. Rotation matrix $\mathbf{R}_P$ can be calculated substituting the values of angles α and β into expression (5). Then the orientation of frame 6 becomes determined. Considering the kinematic chain with universal joint 2–3, the vector $\mathbf{p}_S$ can be represented as follows

$$\mathbf{p}_S = \mathbf{p}_{B1} + \mathbf{s}_1 q_1 + \mathbf{R}_P\left(-\mathbf{r}_{C1}^P + \mathbf{r}_D^P + \mathbf{s}_4^P q_4 + \mathbf{s}_5^P q_5 - \mathbf{n}^P l\right), \quad (17)$$

where $\mathbf{p}_{B1}$ are the coordinates of point B_1, which is the origin of generalized coordinate q_1 in system $OXYZ$; $\mathbf{r}_{C1}^P$ are the coordinates of point C_1 in system $PX_PY_PZ_P$; $\mathbf{r}_D^P$ are the coordinates of point D, which is the origin of generalized coordinate q_4 in system $PX_PY_PZ_P$; $\mathbf{s}_4^P$ and $\mathbf{s}_5^P$ are the unit vectors directed along the axes of prismatic kinematic pairs 6–7 and 8–9 corresponding to generalized coordinates q_4 and q_5 and expressed in system $PX_PY_PZ_P$; l is the length of output element 10 determined by distance KS (Figure 3).

Parameters $\mathbf{p}_{B1}$, $\mathbf{r}_{C1}^P$, $\mathbf{r}_D^P$, $\mathbf{s}_4^P$, $\mathbf{s}_5^P$, and l are determined only by the manipulator's design and are considered as given. Let's expand the brackets in expression (17) and group the components as follows

$$\mathbf{s}_1 q_1 + \mathbf{s}_4 q_4 + \mathbf{s}_5 q_5 = \mathbf{a}, \quad (18)$$

where

$$\begin{gathered} \mathbf{s}_4 = \mathbf{R}_P\mathbf{s}_4^P, \mathbf{s}_5 = \mathbf{R}_P\mathbf{s}_5^P, \\ \mathbf{a} = \mathbf{p}_S - \mathbf{p}_{B1} - \mathbf{R}_P\left(-\mathbf{r}_{C1}^P + \mathbf{r}_D^P - \mathbf{n}^P l\right), \end{gathered} \quad (19)$$

where $\mathbf{s}_4$ and $\mathbf{s}_5$ are the unit vectors directed along the axes of prismatic kinematic pairs 6–7 and 8–9, corresponding to generalized coordinates q_4 and q_5 (Figure 3) and expressed in global system $OXYZ$.

Parameters $\mathbf{s}_4$, $\mathbf{s}_5$, and $\mathbf{a}$ can be calculated according to equation (19) since rotation matrix $\mathbf{R}_P$ of coordinate system $PX_PY_PZ_P$ was determined, and coordinates $\mathbf{p}_S$ of point S are assumed to be given when solving the inverse kinematics. Then expression (18) becomes a relationship with respect to three unknowns—q_1, q_4, and q_5, which can be determined as follows. Let's introduce auxiliary quantities

$$\mathbf{u}_{45} = \mathbf{s}_4 \times \mathbf{s}_5, \mathbf{u}_{15} = \mathbf{s}_1 \times \mathbf{s}_5, \mathbf{u}_{14} = \mathbf{s}_1 \times \mathbf{s}_4. \quad (20)$$

The values of the generalized coordinates q_1, q_4, and q_5 can be found by sequential performing the scalar product of each of the auxiliary values of expression (20) with both sides of relation (18)

$$q_1 = \frac{\mathbf{a}^{\mathrm{T}}\mathbf{u}_{45}}{\mathbf{s}_1^{\mathrm{T}}\mathbf{u}_{45}}, \; q_4 = \frac{\mathbf{a}^{\mathrm{T}}\mathbf{u}_{15}}{\mathbf{s}_4^{\mathrm{T}}\mathbf{u}_{15}}, \; q_5 = \frac{\mathbf{a}^{\mathrm{T}}\mathbf{u}_{14}}{\mathbf{s}_5^{\mathrm{T}}\mathbf{u}_{14}}. \quad (21)$$

Note that the denominator in any of expressions (21) turns to zero if vectors $\mathbf{s}_1$, $\mathbf{s}_4$, and $\mathbf{s}_5$ are in the same plane. Such a relative position of these vectors corresponds to a singular position of the manipulator. Consider next the calculation of two remaining generalized coordinates q_2 and q_3. First, one can find coordinates $\mathbf{p}_P$ of point P relative to system $OXYZ$ as

$$\mathbf{p}_P = \mathbf{p}_{B1} + \mathbf{s}_1 q_1 - \mathbf{R}_P\mathbf{r}_{C1}^P. \quad (22)$$

Then, expressions for coordinates $\mathbf{p}_{Ai}$ and $\mathbf{p}_{Ci}$ of the centers of spherical joints 5–6 and 4–5, that is, points A_i and C_i, $i = 2, 3$ (Figure 3), can be derived in the following form

$$\mathbf{p}_{Ai} = \mathbf{p}_P + \mathbf{R}_P\mathbf{r}_{Ai}^P, \quad (23)$$

$$\mathbf{p}_{Ci} = \mathbf{p}_{Bi} + \mathbf{s}_i q_i, \quad (24)$$

where $\mathbf{r}_{Ai}^P$ are the coordinates of point A_i relative to system $PX_PY_PZ_P$; $\mathbf{p}_{Bi}$ are the coordinates of point B_i, which is the origin of generalized coordinate q_i, in system $OXYZ$; $\mathbf{s}_i$ is the unit vector directed along the axis of the prismatic pair,

corresponding to the direction of generalized coordinate q_i and expressed in system $OXYZ$ (Figure 3).

The coordinates of the centers of spherical joints A_i and C_i are related to each other through length L_{AiCi} of link A_iC_i:

$$(\mathbf{p}_{Ai} - \mathbf{p}_{Ci})^2 = L_{AiCi}^2, i = 2, 3. \quad (25)$$

Let's substitute (23) and (24) in (25) and get quadratic equation relative to q_i after transformations

$$q_i^2 + 2b_i q_i + c_i = 0, i = 2, 3. \quad (26)$$

The calculation of coefficients b_i and c_i is in Appendix 1, formulae (A1) and (A2). In the general case, quadratic equation (26) has two solutions, and the choice of a specific one is determined by the design features of the manipulator. Thus, the values of all five generalized coordinates of the manipulator were determined.

Forward kinematics solution

The solution of the forward position problem for the studied manipulator consists in finding vector $\mathbf{p}_S$, which determines the position of the end-effector, and vector $\mathbf{n}$, which determines its orientation, for given vector of generalized coordinates $\mathbf{q}$. The algorithm for solving this problem can be presented as follows. First, consider the problem of determining the position and orientation of frame 6, that is, parameters $\mathbf{p}_P$ and $\mathbf{R}_P$, for given values of generalized coordinates q_1, q_2, and q_3. Such calculation methodology is similar to the algorithm presented by Li et al.[44] and is as follows. First, coordinates $\mathbf{p}_{Ci}$ of points C_i, $i = 1 \ldots 3$, are determined relative to global coordinate system $OXYZ$ using expression (24). Then, the following expression can be composed considering the closed loops formed by kinematic chain with universal joint 2–3 and kinematic chains with spherical joints 4–5 and 5–6

$$L_{AiCi}\mathbf{w}_i = -\mathbf{p}_{Ci} + \mathbf{p}_{C1} + \mathbf{R}_P(\mathbf{r}_{Ai}^P - \mathbf{r}_{C1}^P), i = 2, 3, \quad (27)$$

where $\mathbf{w}_i$ is the unit vector directed from point C_i to point A_i (Figure 3).

Let's square both sides of expression (27) with respect to expression (5)

$$\mathbf{d}_i^{\mathrm{T}}\mathbf{R}_\alpha\mathbf{R}_\beta\mathbf{e}_i = f_i, i = 2, 3. \quad (28)$$

Formulae (A3) to (A5) given in Appendix 1 allow to calculate parameters $\mathbf{d}_i$, $\mathbf{e}_i$, and f_i. These parameters become known when solving the forward position problem. The system of equation (28) is represented by two equations with two unknown rotational angles α and β in universal joint 2–3. Let's expand expression (28) taking into account the product of rotation matrices $\mathbf{R}_\alpha\mathbf{R}_\beta$ according to (11) and group the parameters with respect to variable β as follows

$$D_i\cos\beta + E_i\sin\beta + F_i = 0, i = 2, 3. \quad (29)$$

Coefficients D_i, E_i, and F_i depend on angle α and can be found in Appendix 1 (formulae (A6) to (A8)). Let's apply the tangent half-angle substitution

$$\begin{aligned} \sin\beta &= \frac{2t_\beta}{1+t_\beta^2}, \cos\beta = \frac{1-t_\beta^2}{1+t_\beta^2}, t_\beta = \tan(\beta/2), \\ \sin\alpha &= \frac{2t_\alpha}{1+t_\alpha^2}, \cos\alpha = \frac{1-t_\alpha^2}{1+t_\alpha^2}, t_\alpha = \tan(\alpha/2), \end{aligned} \quad (30)$$

using which relationship (29) can be written in the following way

$$k_{i2}t_\beta^2 + k_{i1}t_\beta + k_{i0} = 0, i = 2, 3. \quad (31)$$

Coefficients k_{i2}, k_{i1}, and k_{i0} are in the Appendix 1, formulae (A9) to (A11). Further, one can apply dialytic elimination method[45] to determine the solutions of equation system (31). For this purpose, firstly multiply both sides of expression (31) by t_β and rewrite the resulting equation system substituting for $i = 2$ and 3

$$\begin{aligned} k_{22}t_\beta^2 + k_{21}t_\beta + k_{20} &= 0, \\ k_{22}t_\beta^3 + k_{21}t_\beta^2 + k_{20}t_\beta &= 0, \\ k_{32}t_\beta^2 + k_{31}t_\beta + k_{30} &= 0, \\ k_{32}t_\beta^3 + k_{31}t_\beta^2 + k_{30}t_\beta &= 0. \end{aligned} \quad (32)$$

Equation (32) can be presented in matrix form

$$\mathbf{K}\mathbf{t}_\beta = 0, \quad (33)$$

where

$$\mathbf{K} = \begin{bmatrix} 0 & k_{22} & k_{21} & k_{20} \\ k_{22} & k_{21} & k_{20} & 0 \\ 0 & k_{32} & k_{31} & k_{30} \\ k_{32} & k_{31} & k_{30} & 0 \end{bmatrix}, \mathbf{t}_\beta = \begin{bmatrix} t_\beta^3 \\ t_\beta^2 \\ t_\beta \\ 1 \end{bmatrix}. \quad (34)$$

Relationship (33) is a system of linear equations with respect to vector of unknowns $\mathbf{t}_\beta$. The determinant of matrix $\mathbf{K}$ must be equal to zero to have a nontrivial solution for this equation system

$$\det\mathbf{K} = 0. \quad (35)$$

Substituting (34) in (35), we obtain the following equation

$$\begin{aligned} &k_{22}^2k_{30}^2 + k_{32}^2k_{20}^2 + k_{22}k_{31}^2k_{20} + k_{32}k_{21}^2k_{30} - 2k_{22}k_{32}k_{20}k_{30} \\ &-k_{22}k_{21}k_{31}k_{30} - k_{32}k_{31}k_{21}k_{20} = 0. \end{aligned} \quad (36)$$

Since coefficients k_{i2}, k_{i1}, and k_{i0} have the degree of t_α not greater than two, relationship (36) is an octic polynomial equation with respect to variable t_α. This equation will have eight solutions (including complex ones), which can be found, for example, as the eigenvalues of companion matrix for the polynomial on the left side of expression (36).[46]

Variable t_β can be found by multiplying the first equation of system (32) by k_{32}, the third equation by k_{22}, and subtracting them from each other. Finally, the following equation is obtained

$$t_\beta = \frac{k_{22}k_{30} - k_{32}k_{20}}{k_{32}k_{21} - k_{22}k_{31}}. \quad (37)$$

After calculation parameters t_α and t_β, angles α and β can be found using equation (30), and rotation matrix $\mathbf{R}_P$ using (5) to (8). Coordinates $\mathbf{p}_P$ of point P can be calculated through equation (22).

Thus, the position and orientation of frame 6 are determined. The further solution of the forward position problem is as follows: coordinates $\mathbf{p}_S$ of point S of the end-effector can be calculated according to expression (17) and its orientation characterized by vector $\mathbf{n}$ can be calculated using relation (4). Since expression (36) can have up to eight different solutions for parameter α, the several distinct assemblies of the manipulator exist for the same values of the generalized coordinates.

Reachable workspace construction

Several types of workspaces are known for parallel and parallel–serial manipulators [1]: translation, orientation, reachable, dextrous, and others. This study provides an approach to find a reachable workspace, that is, the set of positions, which the end-effector can take with at least one orientation. For the presented manipulator, the reachable workspace corresponds to the set of all possible values of vector $\mathbf{p}_S$ for at least one value of vector $\mathbf{n}$.

Let's consider the following constraints for the presented manipulator, which affect the shape and size of the workspace:

(1) Constraints in actuated kinematic pairs

$$\mathbf{q}_{\min} < \mathbf{q} < \mathbf{q}_{\max}, \quad (38)$$

where $\mathbf{q}_{\min}$ and $\mathbf{q}_{\max}$ are the minimal and maximal value of $\mathbf{q}$.

(2) Constraints in angles of universal joint 2–3

$$\alpha_{\min} < \alpha < \alpha_{\max},\ \beta_{\min} < \beta < \beta_{\max}, \quad (39)$$

where $\alpha_{\min}$, $\beta_{\min}$, $\alpha_{\max}$, and $\beta_{\max}$ are the minimal and maximal values of angles α and β.

(3) Constraints in angles φ_{Ai} and φ_{Ci} in spherical joints 5–6 and 4–5, $i = 2, 3$

$$\varphi_{Ai\,\min} < \varphi_{Ai} < \varphi_{Ai\,\max},\ \varphi_{Ci\,\min} < \varphi_{Ci} < \varphi_{Ci\,\max}, \quad (40)$$

where $\varphi_{Ai\,\min}$, $\varphi_{Ci\,\min}$, $\varphi_{Ai\,\max}$, and $\varphi_{Ci\,\max}$ are the minimal and maximal values of angles φ_{Ai} and φ_{Ci}.

Angle φ_{Ai} can be defined as the angle between vector $\mathbf{w}_i$ and some arbitrarily chosen vector $\mathbf{v}^P$, having a constant value in system $PX_PY_PZ_P$

$$\varphi_{Ai} = \arccos(\mathbf{w}_i^{\mathrm{T}}\mathbf{R}_P\mathbf{v}^P), i = 2, 3. \quad (41)$$

Angle φ_{Ci} can be defined as the angle between vectors $\mathbf{w}_i$ and $\mathbf{s}_i$

$$\varphi_{Ci} = \arccos(\mathbf{w}_i^{\mathrm{T}}\mathbf{s}_i), i = 2, 3. \quad (42)$$

To determine the reachable workspace taking into account the above constraints, the previously obtained algorithms for solving the inverse and forward position problems can be used:

1. Given the values of generalized coordinates q_1, q_2, and q_3 from range (38) and using the approach for solving the forward position problem, it is possible to determine the reachable workspace of point P, the center of frame 6. Since there are theoretically up to eight different assemblies of the manipulator for each combination of q_1, q_2, and q_3, the reachable workspace found at this stage can include several disjoint areas. Coordinates q_1, q_2, and q_3 can be specified by discretization of range (38) with any desired step. The values of angles α and β corresponding to each value of $\mathbf{p}_P$ are also determined at this stage, that is, the orientation of the manipulator's end-effector is also determined.
2. The solutions $\mathbf{p}_P$ for which conditions (39) are not satisfied are excluded.
3. For the remaining values of $\mathbf{p}_P$ and the corresponding values of α and β, coordinates $\mathbf{p}_{Ai}$ of points A_i, $i = 2, 3$, are determined using equations (23) and (5). Also, coordinates $\mathbf{p}_{Ci}$ of points C_i, $i = 2, 3$, for the corresponding values of q_2 and q_3 are determined through equation (24). Given the values of $\mathbf{p}_{Ai}$ and $\mathbf{p}_{Ci}$, vector $\mathbf{w}_i$ can be found, and then conditions (40) can be verified using (41) and (42). Next, it is necessary to exclude those values of $\mathbf{p}_P$ for which these conditions fail. As a result, the reachable workspace for point P of frame 6 is obtained taking into account constraints (38) to (40), as well as the corresponding values of angles α and β.
4. Since point S has two translational DOFs relative to frame 6, the set of its possible positions relative to point P is a plane. The position and orientation of this plane in space is uniquely determined by parameters $\mathbf{p}_P$, α, and β found in the previous stage. Since generalized coordinates q_4 and q_5 have constraints in form (38), the workspace of point S relative to point P is a plane fragment, which is a parallelogram in the

Table 1. Manipulator parameters.

	i		
Parameter	1	2	3
$\mathbf{p}_{Bi}$, mm	$[0\ 324.85\ 0]^T$	$[166.05\ -326.2\ 0]^T$	$[-166.05\ -326.2\ 0]^T$
$\mathbf{r}_{Ai}^P$, mm	–	$[166.05\ -316.05\ -64.5]^T$	$[-166.05\ -316.05\ -64.5]^T$
$\mathbf{r}_{C1}^P$, mm		$[0\ 335\ -110]^T$	
$\mathbf{r}_D^P$, mm		$[0\ 0\ 0]^T$	
L_{AiCi}, mm	–	90	90
l, mm		135.76	
$\mathbf{s}_i$		$[0\ 0\ 1]^T$	
$\mathbf{s}_4^P$		$[0\ 1\ 0]^T$	
$\mathbf{s}_5^P$		$[1\ 0\ 0]^T$	
$\mathbf{n}^P$		$[0\ 0\ 1]^T$	
$\mathbf{u}_1$		$[0\ 1\ 0]^T$	
$\mathbf{R}_P^{C1}$		$\begin{bmatrix} 0 & 1 & 0 \\ -1 & 0 & 0 \\ 0 & 0 & 1 \end{bmatrix}$	

general case. The direction of its sides is determined by vectors $\mathbf{s}_4$ and $\mathbf{s}_5$. The set of such parallelograms, designed for each previously found value of $\mathbf{p}_P$, forms the reachable workspace of the manipulator.

Examples of kinematic problems solution and workspace construction

Consider examples of position problems solution in this section. The geometrical parameters of the manipulator are presented in Table 1, they correspond to the developed CAD model shown in Figure 2.

The following arrangement of coordinate systems is taken in the considered examples. Global coordinate system $OXYZ$ is set in such a way that its origin, point O, is at the geometric center of the plane corresponding to the upper surface of the base. X and Y axes are in the same plane, and X axis is perpendicular to the long side of the base, and Y axis is perpendicular to the short side. Z axis is perpendicular to the base plane and directed upward vertically. Points B_i, $i = 1 \ldots 3$, are in XY plane. The direction of vector $\mathbf{u}_1$ coincides with the positive direction of Y axis. Vectors $\mathbf{s}_i$, $i = 1 \ldots 3$, are directed parallel to Z axis.

Origin P of coordinate system $PX_PY_PZ_P$ is located in the geometric center of the plane corresponding to the top surface of frame 6. X_P and Y_P axes are in the same plane, herewith X_P axis is perpendicular to the long side of frame 6, and Y_P axis is perpendicular to the short side. Z_P axis is perpendicular to the plane of frame 6 and is directed upward. Point D is chosen in such a way that it coincides with point P. Vector $\mathbf{s}_4^P$ is directed along Y_P axis, and vector $\mathbf{s}_5^P$ is directed parallel to X_P. Vector $\mathbf{n}_P$ is perpendicular to the plane of frame 6, and its direction coincides with the positive direction of Z_P axis.

Example of inverse kinematics solution

Consider an example of the inverse kinematics solution. Let's take laws of position $\mathbf{p}_S(t)$ and orientation $\mathbf{n}(t)$ variation of the end-effector in the following form

$$\mathbf{p}_S(t) = \begin{bmatrix} \frac{30\varphi(t)}{2\pi}\cos\varphi(t) \\ \frac{30\varphi(t)}{2\pi}\sin\varphi(t) \\ 240 - \frac{30\varphi(t)}{2\pi} \end{bmatrix} \text{mm}, \mathbf{n}(t) = \begin{bmatrix} \sin\frac{\pi}{12}\cos\varphi(t) \\ \sin\frac{\pi}{12}\sin\varphi(t) \\ \cos\frac{\pi}{12} \end{bmatrix}, \quad (43)$$

$$\varphi(t) = 6\pi t/15 \text{ rad}, t = (0, 15)\text{s}. \quad (44)$$

Such law motions correspond to three revolutions in 15 s of point S along a spiral-helical trajectory, the axis of which coincides with Z axis of global coordinate system $OXYZ$ (Figure 5). The radial step of the curve is equal to the axial one and is 30 mm. At the initial time point, the height of point S above XY plane is 240 mm. In this case, the orientation of the end-effector

changes in such a way that vector **n** rotates around Z axis and forms angle of 15° with this axis during the whole time of movement.

The solution of the inverse position problem according to the developed algorithm was carried out using MATLAB package. The solution results are shown in Figure 6.

It follows from Figure 6 that all five generalized coordinates have an oscillatory nature. Oscillations of generalized coordinates $q_1 - q_3$ are caused by the rotation of output element 10 around Z axis, their amplitude is constant, but the entire oscillation range is shifted, which corresponds to the movement of output element 10 along Z axis. The oscillatory amplitude of generalized coordinates q_4 and q_5 increases, this is due to the spiral motion of point S in the plane parallel to XY plane.

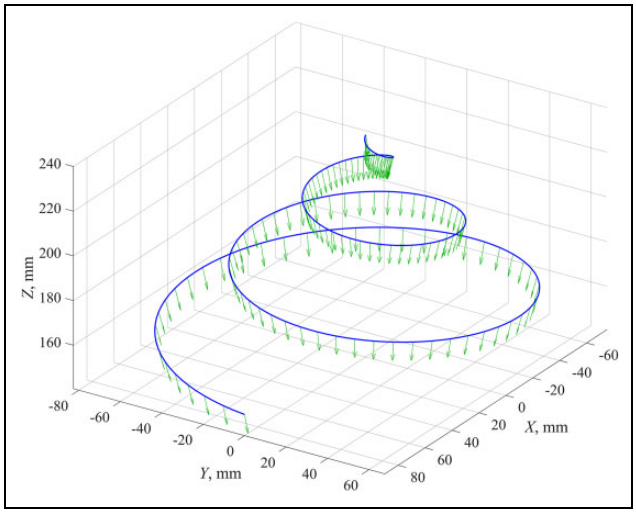

Figure 5. The motion trajectory of the manipulator's end-effector for solving the inverse kinematic problem (arrows show the orientation of output element 10).

Example of forward kinematics solution

Consider an example of the forward kinematics solution. Suppose that the values of the generalized coordinates correspond to the solution of the inverse position problem for laws (43) for certain random time point. For example, for $t = 3.7$ s the following values of the end-effector's coordinates and the corresponding values of the generalized coordinates (accurate to two decimals) are obtained

$$\begin{aligned} \mathbf{p}_S &= [-1.39 \quad -22.16 \quad 217.80]^{\mathrm{T}}\mathrm{mm}, \\ \mathbf{n} &= [-0.02 \quad -0.26 \quad 0.97]^{\mathrm{T}}, \end{aligned} \tag{45}$$

$$\mathbf{q} = [337.29 \quad 126.50 \quad 120.92 \quad -31.08 \quad -3.40]^{\mathrm{T}}\mathrm{mm} \tag{46}$$

The solution of the forward position problem for the values of the generalized coordinates given in (46) was carried out according to the developed algorithm using MATLAB package. Polynomial equation (36) was obtained using symbolic calculations. The solution of this equation was determined using standard function "vpasolve." Solution of equation (36) gave eight values

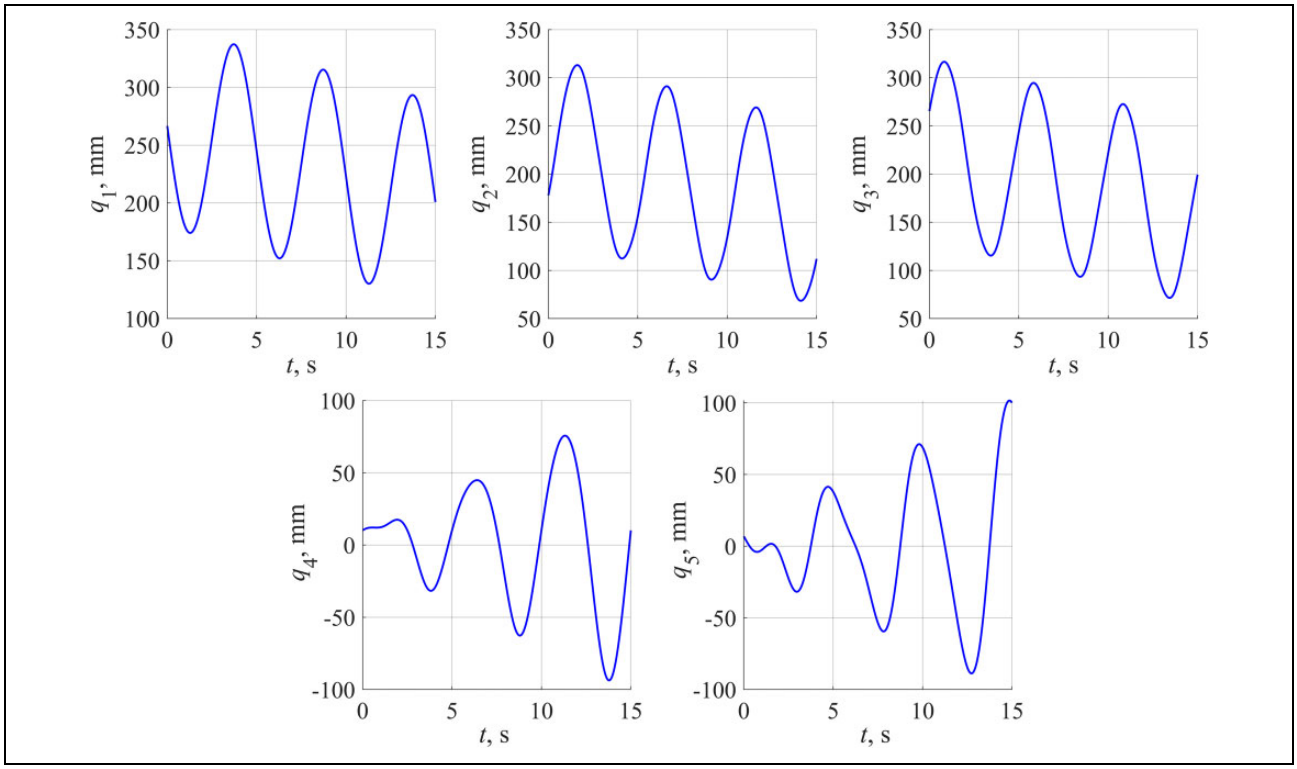

Figure 6. The inverse problem solution when the end-effector moves along the spiral-helical trajectory shown in Figure 5.

of variable t_α, four of which were complex. Further calculations were carried out only for the real values of the variables. Consequently, four groups of values of vectors $\mathbf{p}_S$ and $\mathbf{n}$ were obtained, they are presented in Table 2.

Group of solution II according to Table 2 corresponds to expressions (45). Groups of solution I, III, and IV refer to three other configurations of the manipulator that exist for the same values of the generalized coordinates given in (46). Figure 7 shows the assemblies of the manipulator corresponding to the obtained solutions of the forward position problem given in Table 2.

Table 2. Solution of the forward kinematic problem.[a]

	Group of solution			
Parameter	I	II	III	IV
$\mathbf{p}_S$, mm	$\begin{bmatrix} 48.59 \\ -1.94 \\ 177.47 \end{bmatrix}$	$\begin{bmatrix} -1.39 \\ -22.16 \\ 217.80 \end{bmatrix}$	$\begin{bmatrix} -0.01 \\ 18.36 \\ 135.40 \end{bmatrix}$	$\begin{bmatrix} -53.06 \\ -1.64 \\ 178.28 \end{bmatrix}$
$\mathbf{n}$	$\begin{bmatrix} -0.29 \\ -0.39 \\ 0.87 \end{bmatrix}$	$\begin{bmatrix} -0.02 \\ -0.26 \\ 0.97 \end{bmatrix}$	$\begin{bmatrix} -0.01 \\ -0.49 \\ 0.87 \end{bmatrix}$	$\begin{bmatrix} 0.27 \\ -0.39 \\ 0.88 \end{bmatrix}$

[a]The data are presented accurate to two decimals.

Example of reachable workspace construction

Let's consider an example of reachable workspace construction. Constraint values (38) to (40) correspond to the CAD model of the manipulator shown in Figure 2 and are presented below

$$\begin{gathered} \mathbf{q}_{\min} = [\,140.00 \quad 118.50 \quad 118.50 \quad -252.33 \quad -115.34\,]^{\mathrm{T}}\mathrm{mm}, \\ \mathbf{q}_{\max} = [\,198.00 \quad 169.50 \quad 169.50 \quad 252.33 \quad 115.34\,]^{\mathrm{T}}\mathrm{mm}, \\ \alpha_{\min} = \beta_{\min} = \varphi_{Ai\,\min} = \varphi_{Ci\,\min} = -\pi/6 \text{ rad}, \\ \alpha_{\max} = \beta_{\max} = \varphi_{Ai\,\max} = \varphi_{Ci\,\max} = \pi/6 \text{ rad}. \end{gathered} \tag{47}$$

Unit vector that is perpendicular to the plane of frame 6 (the third column of matrix $\mathbf{R}_P$) was chosen as vector $\mathbf{v}^P$ for the calculation of angle φ_{Ai} according to expression (41).

First, the reachable workspace for point P was determined according to the presented methodology. Calculations were carried out for 10 values of each of coordinates q_1, q_2, and q_3 (1000 different combinations in total), equally distributed within range $[\mathbf{q}_{\min}\ \mathbf{q}_{\max}]$. Four disjoint areas in space were built (Figure 8) in the result of the calculation.

Condition (39) excludes some of the solutions (red areas according to Figure 8), and condition (40) leaves only one feasible solution range (blue area according to Figure 8).

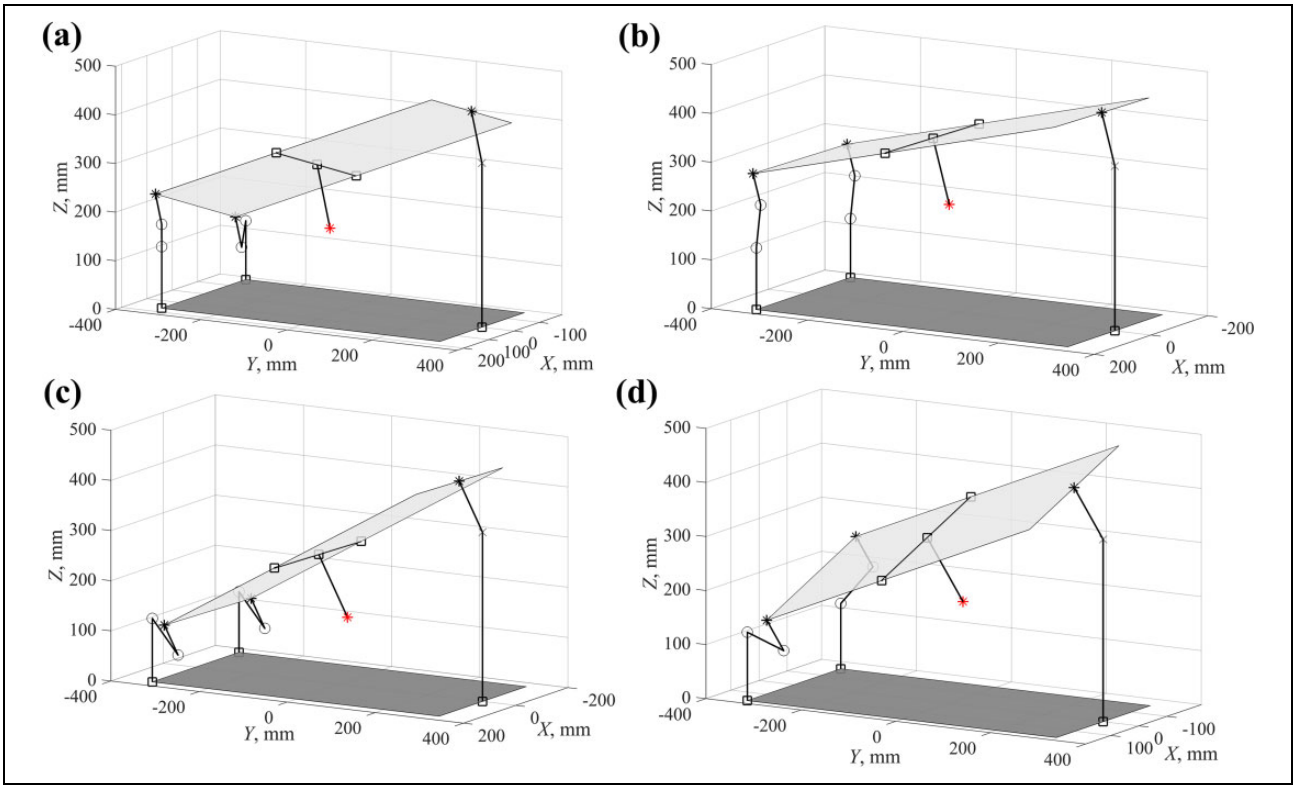

Figure 7. Assemblies of the 5-DOF (3T2R) parallel–serial (hybrid) manipulator obtained in solving forward kinematic problem: (a) to (d) correspond to groups of solutions I to IV presented in Table 2.

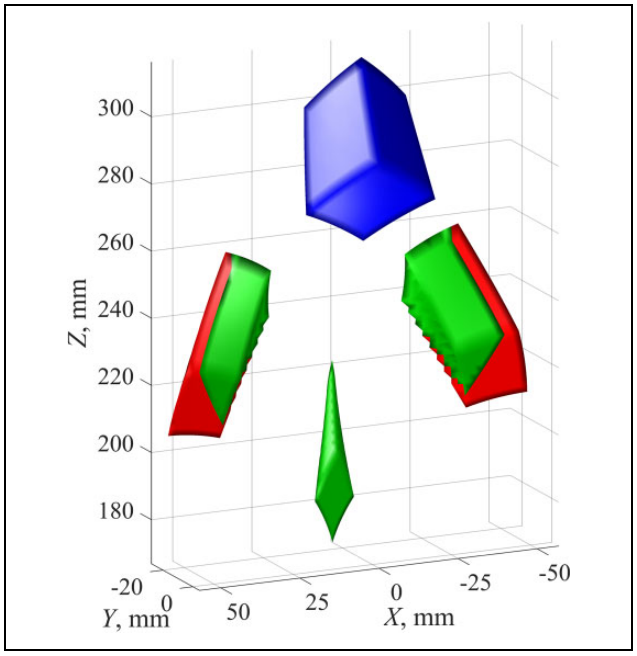

Figure 8. The reachable workspace for point *P*: conditions (39) and (40) are not satisfied in the red and green areas; the blue area satisfies all the requirements.

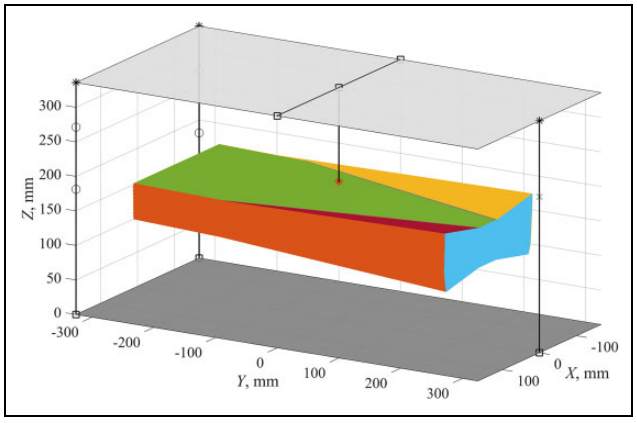

Figure 9. The reachable workspace of the manipulator.

Table 3. Dimensions of the reachable workspace and extreme values of the orientation angles.[a]

	X, mm	*Y*, mm	*Z*, mm	α, deg	β, deg
Min	–119.26	–263.04	103.18	–8.79	–3.08
Max	119.23	243.68	189.01	8.79	6.50

[a]The data are presented accurate to two decimals.

Next, the reachable workspace for point S was determined as a set of planes (Figure 9). The dimensions of the workspace and the extreme values of angles α and β (which describe the orientation of the manipulator's end-effector for a given geometry of links) are given in Table 3. Comparing the dimensions of the two workspaces according to Figures 8 and 9, it is easy to conclude how the use of parallel–serial structure greatly increases the size of the workspace.

Conclusions

Algorithms for solving the inverse and forward position problems and also approach of reachable workspace construction for the 5-DOF parallel–serial (hybrid) manipulator, in which the end-effector has three translational and two rotational DOFs (3T2R motion pattern), are obtained in the present study. The considered manipulator includes a parallel part with three DOFs (1T2R motion pattern) based on a tripod and a serial part with two DOFs (2T motion pattern) based on two carriages displaced in perpendicular directions. This manipulator can find application in solving a wide range of technological problems. In particular, it can be used for processing elements having complex shapes and elements in which the size of one dimension exceeds the size of another.

The kinematic analysis results show that the solution of both inverse and forward position problems can be obtained in an analytical form. When solving the inverse problem, first, the rotation angles in the universal joint are determined based on the given orientation of the end-effector, then the generalized coordinates are calculated. In this case, the existence of several solutions is possible, where the choice of a specific solution is determined by the design features of the manipulator. The solution of the forward position problem is based on the application of dialytic elimination method. Using this method, the solution comes to finding the octic polynomial equation roots. It corresponds to the theoretical existence of eight different configurations of the manipulator for the same values of the generalized coordinates.

An approach to find a reachable workspace for this manipulator was developed based on the proposed algorithms of solving both position problems. This approach takes into account the constraints imposed on the generalized coordinates and on the allowable angles in the universal and spherical joints. First, the reachable workspace is calculated for the parallel part of the manipulator and then for the entire manipulator as a whole system. Examples of calculations using MATLAB package are given for all the proposed approaches.

An example of inverse problem solution corresponded to the movement of the end-effector along a spiral-helical trajectory. The laws of generalized coordinates variation, which are necessary for the realization of the given type of movement, are determined in the results of calculation. An example of forward problem solution is considered for the case when four different assemblies of the manipulator exist at the same given values of the generalized coordinates.

For the given geometry of the manipulator and the prescribed values of the design constraints, the reachable workspace was built. Its shape, dimensions, and also the extreme values of the end-effector orientation angles were determined. The kinematic analysis of the manipulator performed

in this study can serve as a basis for the further analysis of velocities and accelerations. In addition, the singularities that can affect the shape and size of the workspace of the manipulator are of special interest. The determination of such positions is related to the velocity analysis of the manipulator and is the subject of upcoming research.

Declaration of conflicting interests

The author(s) declared no potential conflicts of interest with respect to the research, authorship, and/or publication of this article.

Funding

The author(s) disclosed receipt of the following financial support for the research, authorship, and/or publication of this article: The study was supported by the Russian President Grant according to the research project MK-2781.2019.

ORCID iDs

Anton Antonov https://orcid.org/0000-0002-3928-5440
Alexey Fomin https://orcid.org/0000-0003-4071-8407
Giuseppe Carbone https://orcid.org/0000-0003-0831-8358

References

1. Merlet J-P. *Parallel robots*. Dordrecht: Springer Science & Business Media, Vol. 128, 2006, p. 402.
2. Glazunov VA and Chunichin AY. Development of mechanisms of parallel structure. *J Mach Manuf Reliab* 2014; 43: 211–216.
3. Gomez-Bravo F, Carbone G, and Fortes JC. Collision free trajectory planning for hybrid manipulators. *Mechatronics* 2012; 22(6): 836–851.
4. Ganiev RF, Glazunov VA, and Filippov GS. Urgent problems of machine science and ways of solving them: wave and additive technologies, the machine tool industry, and robot surgery. *J Mach Manuf Reliab* 2018; 47: 399–406.
5. Shahinpoor M. Kinematics of a parallel-serial (hybrid) manipulator. *J Robot Syst* 1992; 9(1): 17–36.
6. Carbone G and Ceccarelli M. A stiffness analysis for a hybrid parallel-serial manipulator. *Robotica* 2004; 22(5): 567–576.
7. Lee MK, Park KW, and Choi BO. Kinematic and dynamic models of hybrid robot manipulator for propeller grinding. *J Robot Syst* 1999; 16(3): 137–150.
8. Tönshoff HK, Grendel H, and Kaak R. Structure and characteristics of the hybrid manipulator Georg V. In: Boër CR, Molinari-Tosatti L, and Smith KS. (eds) *Parallel kinematic machines advanced manufacturing*, London: Springer, 1999, pp. 365–376.
9. Cheng HH. Real-time manipulation of a hybrid serial-and-parallel-driven redundant industrial manipulator. *J Dyn Syst Meas Control* 1994; 116(4): 687–701.
10. Yang G, Chen W, and Ho EHL. Design and kinematic analysis of a modular hybrid parallel-serial manipulator. In: *Proceedings of the 7th international conference on Control, Automation, Robotics and Vision (ICARCV)*, Singapore, 2–5 December 2002, Vol. 1, pp. 45–50.
11. Antonov AV, Chernetsov RA, Ulyanov EE, et al. Use of the chord method for analyzing workspaces of a parallel structure mechanism. In: *IOP conference series: materials science and engineering, ToPME-2019*, Moscow, Russia, 2020, Vol. 747, p. 012079.
12. Park K, Kim T, Lee M, et al. Study on kinematic optimization of a combined parallel-serial manipulator. In: *SICE-ICASE International Joint Conference*, Busan, South Korea, 2006, pp. 1212–1216.
13. Yang G, Chen IM, Yeo SH, et al. Design and analysis of a modular hybrid parallel-serial manipulator for robotised deburring applications. In: Wang L and Xi J (eds) *Smart devices and machines for advanced manufacturing*. London: Springer, 2008, pp. 167–188.
14. Nasseri MA, Eder M, Eberts D, et al. Kinematics and dynamics analysis of a hybrid parallel-serial micromanipulator designed for biomedical applications. In: *Proceedings of IEEE/ASME International Conference on Advanced Intelligent Mechatronics*, Wollongong, Australia, 9–12 July 2013, pp. 293–299.
15. Zhou M, Yu Q, Huang K, et al. Towards robotic-assisted subretinal injection: a hybrid parallel–serial robot system design and preliminary evaluation. *IEEE Trans Ind Electron* 2020; 67(8): 6617–6628.
16. Lai YL, Liao CC, and Chao ZG. Inverse kinematics for a novel hybrid parallel–serial five-axis machine tool. *Robot Comput Integr Manuf* 2018; 50: 63–79.
17. Yan C, Gao F, and Zhang Y. Kinematic modeling of a serial–parallel forging manipulator with application to heavy-duty manipulation. *Mech Based Des Struct Mach* 2010; 38(1): 105–129.
18. Daihong C, Guanghua Z, and Rong L. Design of a 6-DOF compliant manipulator based on serial-parallel architecture. In: *Proceedings of IEEE/ASME international conference on advanced intelligent mechatronics*, Monterey, CA, 24–28 July 2005, pp. 765–770.
19. Moosavian SAA, Pourreza A, and Alipour K. Kinematics and dynamics of a hybrid serial-parallel mobile robot. In: *Proceedings of IEEE international conference on robotics and automation (ICRA)*, Kobe, Japan, 12–17 May 2009, pp. 1358–1363.
20. Pinskier J, Shirinzadeh B, Clark L, et al. Development of a 4-DOF haptic micromanipulator utilizing a hybrid parallel-serial flexure mechanism. *Mechatronics* 2018; 50: 55–68.
21. Wang R, Ding G, and Zhong SS. Kinematics analysis of a new 5 DOF parallel-serial machine tool based on the vector method. *Key Eng Mater* 2011; 450: 283–287.
22. Oba Y and Kakinuma Y. Simultaneous tool posture and polishing force control of unknown curved surface using serial-parallel mechanism polishing machine. *Precis Eng* 2017; 49: 24–32.
23. Li Y, Wang L, Chen B, et al. Optimization of dynamic load distribution of a serial-parallel hybrid humanoid arm. *Mech Mach Theory* 2020; 149: 103792.
24. Kanaan D, Wenger P, and Chablat D. Kinematic analysis of a serial–parallel machine tool: the VERNE machine. *Mech Mach Theory* 2009; 44(2): 487–498.

25. Fajardo-Pruna M, Lopez-Estrada L, Perez H, et al. Analysis of a single-edge micro cutting process in a hybrid parallel-serial machine tool. *Int J Mech Sci* 2019; 151: 222–235.
26. Liu R and Yao Y. A novel serial–parallel hybrid worm-like robot with multi-mode undulatory locomotion. *Mech Mach Theory* 2019; 137: 404–431.
27. Romdhane L. Design and analysis of a hybrid serial-parallel manipulator. *Mech Mach Theory* 1999; 34(7): 1037–1055.
28. Huang MZ and Ling S-H. Kinematics of a class of hybrid robotic mechanisms with parallel and series modules. In: *Proceedings of IEEE international conference on robotics and automation (ICRA)*, San Diego, CA, 8–13 May 1994, pp. 2180–2185.
29. Zanganeh KE and Angeles J. Displacement analysis of a six-degree-of-freedom hybrid hand controller. In: *Proceedings of IEEE international conference on robotics and automation (ICRA)*, Minneapolis, MN, 22–28 April 1996, Vol. 2, pp. 1281–1286.
30. Tanev TK. Kinematics of a hybrid (parallel–serial) robot manipulator. *Mech Mach Theory* 2000; 35(9): 1183–1196.
31. Zheng XZ, Bin HZ, and Luo YG. Kinematic analysis of a hybrid serial-parallel manipulator. *Int J Adv Manuf Technol* 2004; 23: 925–930.
32. Dyashkin-Titov VV, Zhoga VV, Nesmiyanov IA, et al. Dynamics of the manipulator parallel-serial structure. In: Evgrafov AN (ed) *Advances in mechanical engineering. lecture notes in mechanical engineering*. Cham, Switzerland: Springer, 2018, pp. 33–43.
33. Gallardo-Alvarado J. Kinematics of a hybrid manipulator by means of screw theory. *Multibody Syst Dyn* 2005, 14: 345–366.
34. Hu B, Yu J, Lu Y, et al. Statics and stiffness model of serial-parallel manipulator formed by k parallel manipulators connected in series. *ASME J Mech Robot* 2012; 4(2): 021012.
35. Bandyopadhyay S and Ghosal A. Analytical determination of principal twists in serial, parallel and hybrid manipulators using dual vectors and matrices. *Mech Mach Theory* 2004; 39(12): 1289–1305.
36. Zhang D, Xu Y, Yao J, et al. Design of a novel 5-DOF hybrid serial-parallel manipulator and theoretical analysis of its parallel part. *Robot Comput Integr Manuf* 2018; 53: 228–239.
37. Wang K, Luo M, Mei T, et al. Dynamics analysis of a three-DOF planar serial-parallel mechanism for active dynamic balancing with respect to a given trajectory. *Int J Adv Robot Syst* 2013; 10(23): 1–10.
38. Zeng Q and Fang Y. Structural synthesis of serial-parallel hybrid mechanisms based on representation and operation of logical matrix. *J Mech Robot* 2009; 1(4): 041003.
39. Milutinovic M, Slavkovic N, and Milutinovic D. Kinematic modeling of hybrid parallel serial five-axis machine tool. *Fme Transactions* 2013; 41: 1–10.
40. Fan KC, Wang H, Zhao JW, et al. Sensitivity analysis of the 3-PRS parallel kinematic spindle platform of a serial-parallel machine tool. *Int J Mach Tool Manufact* 2003; 43(15): 1561–1569.
41. Zhang Z and Meng G. Design and analysis of a six degrees of freedom serial–parallel robotic mechanism with multi-degree of freedom legs. *Int J Adv Robot Syst* 2018; 15(8): 1–14.
42. Lu Y, Chang Z, and Ye N. Forward acceleration of kinematic limbs for redundant serial–parallel manipulators. *J Mech Robot* 2020; 12(1): 014502.
43. Ibrahim O and Khalil W. Inverse dynamic modeling of serial-parallel hybrid robots. In: *Proceedings of IEEE/RSJ international conference on intelligent robots and systems*, Beijing, China, 9–15 October 2006, pp. 2156–2161.
44. Li M, Huang T, Chetwynd DG, et al. Forward position analysis of the 3-DOF module of the TriVariant: a 5-DOF reconfigurable hybrid robot. *J Mech Des* 2006; 128(1): 319–322.
45. Roth B. Computations in kinematics. In: Angeles J, Hommel G, and Kovacs P (eds) *Computational kinematics. Solid mechanics and its applications*, Vol. 28. Dordrecht: Springer, 1993, pp. 3–14.
46. Niu X-M and Sakurai T. A method for finding the zeros of polynomials using a companion matrix. *Japan J Indust Appl Math* 2003; 20(2): 239–256.

Appendix 1

$$b_i = \mathbf{s}_i^{\mathrm{T}}(\mathbf{p}_{Bi} - \mathbf{p}_{Ai}), \tag{A1}$$

$$c_i = (\mathbf{p}_{Bi} - \mathbf{p}_{Ai})^2 - L_{AiCi}^2, \tag{A2}$$

$$\mathbf{d}_i = [\,d_{ix} \quad d_{iy} \quad d_{iz}\,]^{\mathrm{T}} = 2\mathbf{R}_{C1}^{\mathrm{T}}(\mathbf{p}_{C1} - \mathbf{p}_{Ci}), \tag{A3}$$

$$\mathbf{e}_i = [\,e_{ix} \quad e_{iy} \quad e_{iz}\,]^{\mathrm{T}} = \mathbf{R}_P^{C1}\left(\mathbf{r}_{Ai}^P - \mathbf{r}_{C1}^P\right), \tag{A4}$$

$$f_i = L_{AiCi}^2 - (\mathbf{p}_{C1} - \mathbf{p}_{Ci})^2 - \left(\mathbf{r}_{Ai}^P - \mathbf{r}_{C1}^P\right)^2, \tag{A5}$$

$$D_i = d_{iz}e_{iz}\cos\alpha - d_{iy}e_{iz}\sin\alpha + d_{ix}e_{ix}, \tag{A6}$$

$$E_i = -\,d_{iz}e_{ix}\cos\alpha + d_{iy}e_{ix}\sin\alpha + d_{ix}e_{iz}, \tag{A7}$$

$$F_i = d_{iy}e_{iy}\cos\alpha + d_{iz}e_{iy}\sin\alpha - f_i, \tag{A8}$$

$$\begin{aligned} k_{i2} = {} & \left(-d_{ix}e_{ix} - d_{iy}e_{iy} + d_{iz}e_{iz} - f_i\right)t_\alpha^2 \\ & + 2\left(d_{iy}e_{iz} + d_{iz}e_{iy}\right)t_\alpha - d_{ix}e_{ix} + d_{iy}e_{iy} \\ & - d_{iz}e_{iz} - f_i, \end{aligned} \tag{A9}$$

$$\begin{aligned} k_{i1} = {} & 2(d_{ix}e_{iz} + d_{iz}e_{ix})t_\alpha^2 + 4d_{iy}e_{ix}t_\alpha \\ & + 2(d_{ix}e_{iz} - d_{iz}e_{ix}), \end{aligned} \tag{A10}$$

$$\begin{aligned} k_{i0} = {} & \left(d_{ix}e_{ix} - d_{iy}e_{iy} - d_{iz}e_{iz} - f_i\right)t_\alpha^2 \\ & + 2\left(-d_{iy}e_{iz} + d_{iz}e_{iy}\right)t_\alpha + d_{ix}e_{ix} + d_{iy}e_{iy} \\ & + d_{iz}e_{iz} - f_i. \end{aligned} \tag{A11}$$